

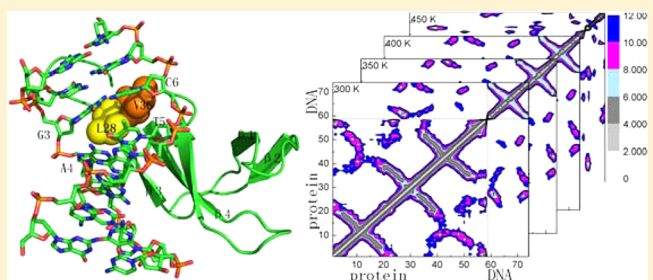
# Influence of Hyperthermophilic Protein Cren7 on the Stability and Conformation of DNA: Insights from Molecular Dynamics Simulation and Free Energy Analysis

Lin Chen, Ji-Long Zhang, Li-Ying Yu, Qing-Chuan Zheng,\* Wen-Ting Chu, Qiao Xue, Hong-Xing Zhang,\* and Chia-Chung Sun

State Key Laboratory of Theoretical and Computational Chemistry, Institute of Theoretical Chemistry, Jilin University, Changchun 130023, People's Republic of China

## S Supporting Information

**ABSTRACT:** Cren7, a novel chromatin protein highly conserved among crenarchaea, plays an important role in genome packaging and gene regulation. However, the detail dynamical structural characteristic of the Cren7–DNA complex and the detail study of the DNA in the complex have not been done. Focused on two specific Cren7–DNA complexes (PDB codes 3LWH and 3LWI), we applied molecular dynamics (MD) simulations at four different temperatures (300, 350, 400, and 450 K) and the molecular mechanics Poisson–Boltzmann surface area (MM-PBSA) free energy calculation at 300 and 350 K to examine the role of Cren7 protein in enhancing the stability of DNA duplexes via protein–DNA interactions, and to study the structural transition in DNA. The simulation results indicate that Cren7 stabilizes DNA duplex in a certain temperature range in the binary complex compared with the unbound DNA molecules. At the same time, DNA molecules were found to undergo B-like to A-like form transitions with increased temperature. The results of statistical analyses of the H-bond and hydrophobic contacts show that some residues have significant influence on the structure of DNA molecules. Our work can give important information to understand the interactions of proteins with nucleic acids and other ligands.



## 1. INTRODUCTION

Interactions between proteins and other biological molecules, especially nucleic acids, are the foundation of many key biological functions such as transcription, translation, replication, and recombination.<sup>1,2</sup> Understanding the protein–DNA interaction has contributed to elucidate mechanisms of protein function and is the central issue of modern molecular biology.<sup>3,4</sup> Hyperthermophilic Crenarchaeota has a variety of abundant, sequence-independent DNA-binding proteins, which are able to compact DNA and play a vital role in DNA stabilization at high growth temperatures.<sup>5–9</sup> These proteins are characteristic of extreme thermal, acid, and chemical stability as well as DNA binding properties.<sup>10</sup> Such proteins have attracted much interest not only for the academic research but also to the industrial applications.<sup>11,12</sup> Many investigators have made great efforts to understand the structure, evolution, hyperthermophilic mechanism, and protein stability.<sup>13–17</sup>

Cren7, a nonspecific DNA-binding protein discovered in *Sulfolobus shibate*, belongs to a novel family of chromatin proteins highly conserved in the crenarchaeota.<sup>18</sup> Cren7 protein bears significant resemblance in both structure and biochemical properties to Sul7 (Sac7d and Sso7d), which has been extensively investigated,<sup>19–24</sup> although the two proteins are unrelated at the amino acid sequence level.<sup>18,25</sup> The 6.6 kDa

Cren7 protein is abundant in hyperthermophilic crenarchaeon *Sulfolobus solfataricus*, binds to DNA without obvious sequence preference, and significantly increases the melting temperature of dsDNA against thermal denaturation.<sup>18</sup> The 3D structures of Cren7–DNA complexes have been determined by X-ray crystallography (PDB codes 3LWH and 3LWI).<sup>26</sup> These two Cren7–DNA complex structures, illustrated in Figure 1, show that the Cren7 protein binds DNA nonspecifically in the minor groove of DNA and causes a single-step sharp kink of about 53° in the DNA double helix through the intercalation of the hydrophobic side chains of Leu28.<sup>26</sup> It is recognized that the conformation of interacting partners undergoes a significant conformational change upon binding. In addition, structural studies and mutational data show that several residues play a critical role in stabilizing the protein–DNA complex by hydrogen bonds and hydrophobic interactions.<sup>18,26,27</sup> These studies can provide plentiful atomic-level structural information to understand protein–DNA interaction, and have given insights into the roles of individual residues in Cren7–DNA

Received: June 14, 2012

Revised: September 25, 2012

Published: September 26, 2012

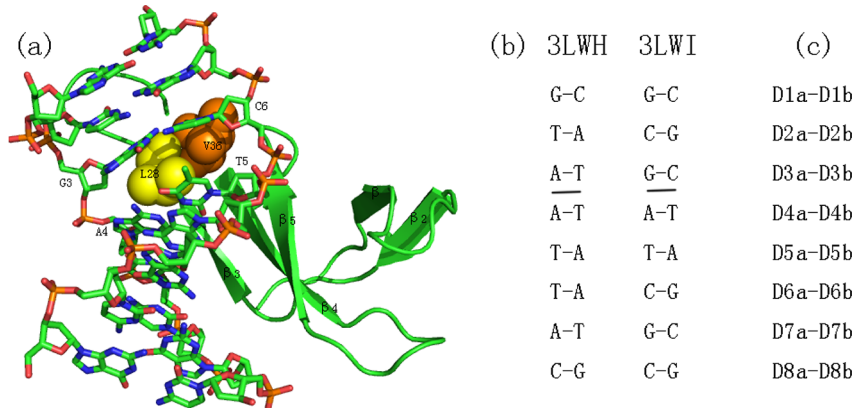


**Figure 1.** (a) The Cren7–DNA complex (PDB ID: 3LWI). Cren7 is given in the cartoon representation, and the intercalating residues L28 and V36 are given in the sphere representation. The kinking sites in the DNA are marked in G3, A4, T5, and C6. (b) The two DNA sequences in 3LWH and 3LWI. The interaction sites in these two sequences are marked by black lines. (c) The representation of the two DNA sequences in part b.

interactions, but the molecular details of the interaction and energetic information at an atomic level are still unclear.

In our work, we used molecular dynamics (MD) simulations and molecular mechanics/Poisson–Boltzmann surface area (MM-PBSA) approach in order to characterize and explore the role of Cren7 protein in enhancing the stabilization of DNA duplexes via protein–DNA interactions. First, MD simulations were carried out for six molecular systems (two complexes of Cren7 protein with different DNA sequences, two unbound DNA, and two unbound protein) from crystal structures at four different temperatures (300, 350, 400, and 450 K) to obtain dynamic structural information. And then, the MM-PBSA approach<sup>28–32</sup> was applied to calculate the binding free energies and nonspecific recognition interactions of two Cren7–DNA complexes, as well as to understand the detailed interaction profile. In addition, the contribution of individual residues to the overall binding free energy was evaluated by decomposing the total binding free energy into individual residues. Thus we can obtain detailed binding energy such as the contribution of individual residues on the binding surface. The detailed interaction profile from MD simulation and MM-PBSA calculation can provide dynamic structural information and energetic information, which are often inaccessible in the static crystal structure. And these characteristics can help us to better understand the interaction of Cren7–DNA. During this study, we have specifically focused on the following: (1) characterizing the ability of Cren7 protein in enhancing the stabilization of DNA duplexes via protein–DNA interactions, (2) calculating binding free energies for the two Cren7–DNA complexes, and (3) elucidating potential amino acid residues involved in interactions with the DNA.

## 2. METHODS

**2.1. Molecular Dynamics Simulations.** The initial crystal structures of Cren7–dsDNA complexes for an AT-rich protein–DNA complex Cren7–d(GTAATTAC)<sub>2</sub> (PDB code: 3LWH) and a GC-rich protein–DNA complex Cren7–d(GCGATCGC)<sub>2</sub> (PDB code: 3LWI)<sup>26</sup> in this study were taken from the Protein Data Bank. The MD simulations including the energy minimization were performed by using AMBER 10 software package<sup>33</sup> and the ff03 force field.<sup>34,35</sup> To keep the whole system neutral, sodium ions ( $\text{Na}^+$ ) or chloride ions ( $\text{Cl}^-$ ) were added by using the xLEAP module in AMBER based on a coulomb potential grid. Each system was then

solvated with the TIP3P water model<sup>36</sup> in a truncated octahedron box with a 10 Å distance around the solute. The protein/DNA were fixed with a 50 kcal mol<sup>-1</sup> Å<sup>-2</sup> constrain, and both solvent and ions were energy minimized for 1500 steps of steepest descent (SD) method followed by a further 3000 steps of conjugate gradient algorithms for each system. Subsequently, these initial harmonic restraints were gradually reduced to zero during a series of progressive energy minimizations. After that, the systems were minimized by the SD method switched to conjugate gradient every 5000 steps totally for 10 000 steps without harmonic restraints. Thereafter, the systems were gently heated from 100 K to the final temperature (300, 350, 400, and 450 K), applying harmonic restraints with a force constant of 5 kcal mol<sup>-1</sup> Å<sup>-2</sup> on the solute atoms, and then equilibrated for 500 ps. Finally, production MD simulations were then carried out for 30 ns except for the systems at 350 K for which 50 ns simulations were performed to check the stability of the simulations. During the minimizations and MD simulations, the particle mesh Ewald summation method<sup>37</sup> was applied to treat the long-range electrostatic interactions with a periodic boundary condition. All bonds involving hydrogen atoms were restricted by the SHAKE algorithm.<sup>38</sup> The time step in all MD simulations was 2 fs. The data given in the tables and figures were obtained from the last 20 ns of the MD simulations unless otherwise mentioned. The PyMOL<sup>39</sup> and VMD software<sup>40</sup> were used to visualize the trajectories and to depict structural representations.

**2.2. MM-PBSA Calculations.** The MM-PBSA method<sup>41–43</sup> using a triplet-trajectory analysis was carried out to calculate the binding free energies for the two Cren7–DNA complexes. For each of the six systems (two complexes, two proteins, and two DNA molecules), 1000 snapshots were extracted from the last 10 ns along the MD trajectories at an interval of 10 ps. The MM-PBSA method and the nmode module implemented in Amber11<sup>44</sup> were employed to estimate the binding free energies. In this method, the binding free energies ( $\Delta G_{\text{bind}}$ ) are computed by the following equations:

$$\Delta G_{\text{bind}} = G_{\text{complex}} - G_{\text{protein}} - G_{\text{DNA}} \quad (1)$$

Here,  $G_{\text{complex}}$ ,  $G_{\text{protein}}$ , and  $G_{\text{DNA}}$  are the free energies of complex, protein, and DNA, respectively. The free energy ( $G_{x=\text{complex,protein,DNA}}$ ) of each species can be estimated by using the MM-PBSA methods:

**Table 1.** Average RMSD Values ( $\text{\AA}$ ) of the Proteins, the Protein–DNA Binary Complexes, and the DNA Structures with Respect to the X-ray Crystal Structures and Canonical A- and B-DNA

	300 K	350 K	400 K	450 K
3LWH				
protein–DNA	1.44 $\pm$ 0.015	2.33 $\pm$ 0.27	2.78 $\pm$ 0.41	3.91 $\pm$ 0.64
protein(complex)	0.89 $\pm$ 0.14	1.06 $\pm$ 0.19	1.69 $\pm$ 0.47	2.10 $\pm$ 0.38
DNA(complexed)-xtal	1.85 $\pm$ 0.27	3.21 $\pm$ 0.62	3.52 $\pm$ 0.63	5.26 $\pm$ 1.13
DNA(complex)-B-form	4.35 $\pm$ 0.19	6.01 $\pm$ 0.36	6.07 $\pm$ 0.47	6.80 $\pm$ 0.99
DNA(complex)-A-form	3.10 $\pm$ 0.25	4.34 $\pm$ 0.38	4.36 $\pm$ 0.59	5.58 $\pm$ 0.99
DNA(alone)-xtal	4.06 $\pm$ 0.40	4.69 $\pm$ 0.61	9.06 $\pm$ 1.76	20.47 $\pm$ 7.36
DNA(alone)-B-form	3.39 $\pm$ 0.26	4.72 $\pm$ 0.51	8.62 $\pm$ 1.70	21.29 $\pm$ 8.04
DNA(alone)-A-form	5.23 $\pm$ 0.42	6.18 $\pm$ 0.56	9.36 $\pm$ 1.45	19.91 $\pm$ 7.22
protein(alone)	1.41 $\pm$ 0.37	1.91 $\pm$ 0.28	2.55 $\pm$ 0.44	3.25 $\pm$ 0.64
3LWI				
protein–DNA	1.50 $\pm$ 0.18	1.81 $\pm$ 0.27	2.15 $\pm$ 0.44	3.63 $\pm$ 0.32
protein(complex)	1.13 $\pm$ 0.19	1.27 $\pm$ 0.24	1.75 $\pm$ 0.42	1.97 $\pm$ 0.29
DNA(complexed)-xtal	1.70 $\pm$ 0.28	2.24 $\pm$ 0.45	3.72 $\pm$ 0.88	9.44 $\pm$ 0.92
DNA(complex)-B-form	5.19 $\pm$ 0.31	5.70 $\pm$ 0.32	5.68 $\pm$ 0.49	9.51 $\pm$ 0.50
DNA(complex)-A-form	2.85 $\pm$ 0.33	3.28 $\pm$ 0.37	3.95 $\pm$ 0.74	8.22 $\pm$ 0.84
DNA(alone)-xtal	3.98 $\pm$ 0.49	4.81 $\pm$ 0.72	6.09 $\pm$ 0.68	9.64 $\pm$ 1.68
DNA(alone)-B-form	2.28 $\pm$ 0.49	3.28 $\pm$ 0.51	4.24 $\pm$ 0.99	9.42 $\pm$ 1.47
DNA(alone)-A-form	4.39 $\pm$ 0.55	4.97 $\pm$ 0.59	6.12 $\pm$ 0.57	10.37 $\pm$ 2.01
protein(alone)	1.56 $\pm$ 0.36	2.27 $\pm$ 0.33	2.39 $\pm$ 0.50	2.80 $\pm$ 0.50

$$G_{x=\text{complex,protein,DNA}} = E_{\text{MM}} + G_{\text{solv}} - TS \quad (2)$$

$$E_{\text{MM}} = E_{\text{ele}} + E_{\text{vdw}} + E_{\text{int}} \quad (3)$$

$$G_{\text{solv}} = G_{\text{pb}} + G_{\text{nonp}} \quad (4)$$

Here,  $E_{\text{MM}}$  is the gas phase molecular mechanical energy,  $G_{\text{solv}}$  is the solvation free energy, and  $E_{\text{ele}}$ ,  $E_{\text{vdw}}$ , and  $E_{\text{int}}$  are the electrostatic energy, the van der Waals interaction energy, and the internal energy, respectively. The solvation free energy,  $G_{\text{solv}}$ , can be computed as the sum of electrostatic solvation energy ( $G_{\text{pb}}$ ) and nonelectrostatic solvation energy ( $G_{\text{nonp}}$ ). The polar component (the electrostatic solvation energy) is computed by using the Poisson–Boltzmann (PB)<sup>45,46</sup> in Amber 11. The dielectric constants were set to 1 and 80<sup>47,48</sup> for the solute and the surrounding solvent respectively in our calculations, and the ionic strength was set to 0.1 M. The nonpolar contribution (the nonelectrostatic solvation energy) is estimated by the equation:

$$G_{\text{nonp}} = \gamma \text{SASA} + \beta \quad (5)$$

Here, the  $\gamma$  and  $\beta$ , two empirical constants, were set as 0.00542 kcal mol<sup>-1</sup> Å<sup>-2</sup> and 0.92 kcal mol<sup>-1</sup>,<sup>49,50</sup> respectively; and SASA is the solvent accessible surface area determined by a probe radius of 1.4 Å. The solute entropy  $S^{\ddagger}$  is estimated by normal-mode analysis, using the normal mode analysis<sup>52</sup> implemented in the Amber11. We took 50 snapshots from the last 10 ns trajectory at an interval of 200 ps to calculate the entropy contribution.

### 3. RESULTS AND DISCUSSION

**3.1. Structural and Dynamic Properties of the Two Cren7–DNA Complexes.** To explore the specific structural changes of the binary complexes, the average root-mean-square deviations (RMSD) of the backbone atoms referenced to the corresponding starting structures are calculated (Table 1). The average RMSD values for the two Cren7 complexes at 300 K are 1.44 Å in 1LWH and 1.50 Å in 1LWI, indicating good agreement with the X-ray crystal structures. However, the

relatively larger average values were obtained at the other three high temperatures (350, 400, and 450 K), implying that the structures of the two Cren7–DNA complexes undergo constant evolution at high temperatures. Moreover, the mean RMSD values of the protein in the two complexes are small with values from 0.89 to 2.10 Å in all of the eight MD simulations. Obviously, there are no remarkable changes for Cren7 protein in the time scale of the simulations. However, similar calculations for the DNA within the two complexes show that the DNA molecules exhibit larger deviations in the two complexes. In a word, the large deviations of the two complexes originate from the instabilities of the DNA double helix. In addition, the DNA in the two complexes displays a smaller fluctuation along the simulations than the free DNA at the same temperature (Figure S1). This fluctuation leads us to conclude the Cren7 protein can enhance the thermal stability of DNA via protein–DNA interactions. The ability of Cren7 in stabilizing the bound DNA molecules will be discussed in some section later. Furthermore, we calculated the RMSD values of the DNA in MD simulations of DNA alone and protein–DNA complexes versus the canonical A- and B-DNA of the same sequence to explore the influence of the Cren7 protein on the bending of the DNA (Table 1). These values indicate that the two DNA molecules in the complexes are closer to the A-DNA than to the B-DNA, while the free DNA molecules are visa versa. These deviations are likely to result from the kink of DNA by the intercalation of the side chains of L28 in Cren7, which is in agreement with the study of Zhang et al.<sup>26</sup> The structure of free Cren7 protein exhibits marginally larger deviations compared with the protein in complexes at the corresponding temperature, but this protein does not undergo major structural transitions in the time scale of the simulations. These changes can be seen from the evolution of Cren7 protein at 450 K (Figure S2).

To illustrate intermolecular and intramolecular interactions in the protein–DNA complexes, the contact maps were drawn by calculating the averages of the inter-residue/nucleotide distances at four different temperatures. There are gradual

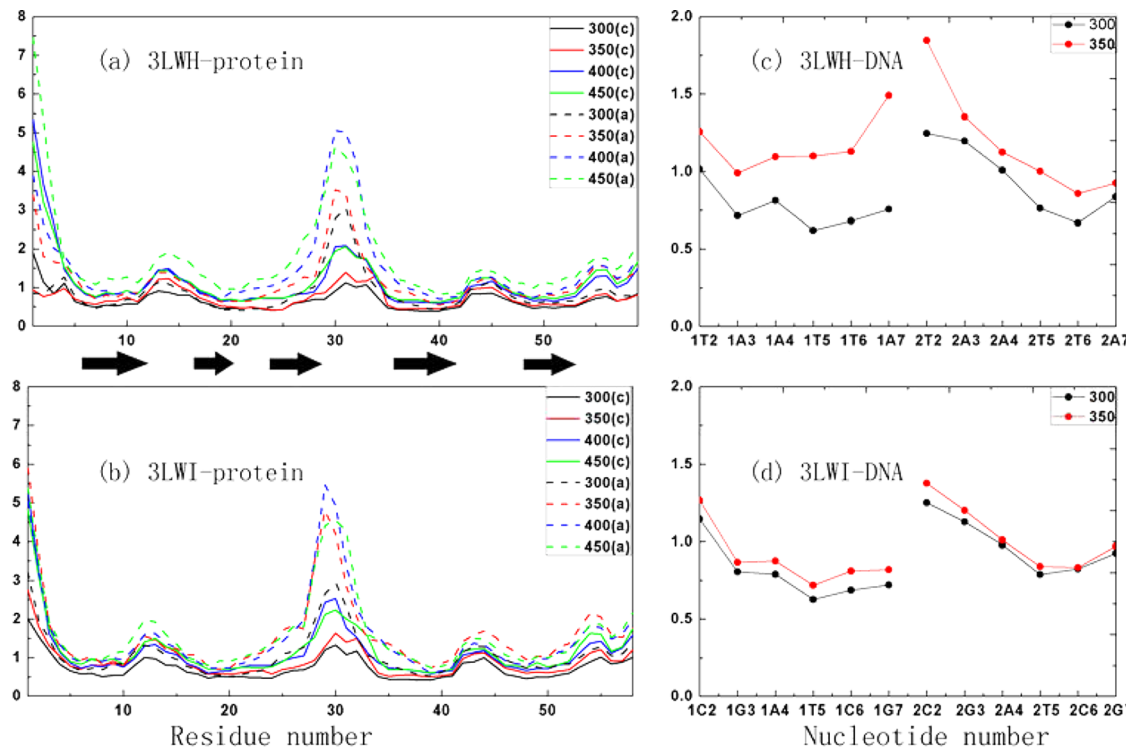


**Figure 2.** The RMSF per residues of protein (a and c) and nucleotides of the DNA (b and d) based on the average structure, using the last 20 ns of the MD simulations. The RMSF values of free protein and protein/DNA in complex were shown with the dashed lines and filled lines, respectively. The  $\beta$ -stands are represented by gray block arrows.

changes in the interactions of protein–DNA and the base pairing in DNA in the two complexes with increasing temperature (Figure S3). Especially, in the simulations at the high temperature of 450 K, the base-pairing in DNA and the protein–DNA contacts are diminished. However, there is no obvious change in the intramolecular interactions of the protein. It is consistent with our previous analysis that the protein retains its initial structure at 450 K in the time scale of the simulations. On the basis of the above analysis, we can deduce that the structure of Cren7 protein in the two complexes is less affected during the four temperature simulations.

Furthermore, the mobility of structural elements in the free Cren7 protein and the two protein–DNA complexes was studied. This was achieved by computing the root-mean-square fluctuations (RMSF) of the protein  $C\alpha$  and DNA backbone atoms with respect to the average coordinates of the last 20 ns MD trajectories. Panels a and b of Figure 2 show the RMSF values for free Cren7 protein and Cren7 protein in the two complexes. The flexibility patterns of the protein residues in the protein–DNA complexes are similar to those obtained from the free protein system. However, MD simulations of the protein in complexes show little fluctuation, especially the loop  $\beta_3\text{--}\beta_4$  (between residue 29 and residue 35) in protein–DNA complexes. It is closer to the DNA-binding site and has low flexibility compared to the corresponding residues in the free protein structure. Reduction of RMSF values of loop  $\beta_3\text{--}\beta_4$  upon DNA binding confirms the existence of interaction between recognition loop and DNA. These explanations are in agreement with the analysis of crystal structures.<sup>26</sup> Panels c and d of Figure 2 show the RMSF values of DNA molecules in the two complexes. Since the base pairings in the DNA molecules are unstable at the high temperatures, the RMSF data from two

high temperature (400 and 450 K) MD simulations are not calculated. Additionally, the RMSF values of the terminal base pairs are not computed due to the end effects. In our simulations, the terminal nucleotides of the duplexes are more flexible than the central nucleotides at the same temperature, as the terminal base pairs are apt to base opening. The nucleotides of the DNA molecules show significantly different flexibility patterns in 3LWH and 3LWI. This may be related to the observation that the Cren7 protein binds asymmetrically to the duplex DNA. Further investigation of the structure of the DNA indicates that the Cren7 protein is capable of stabilizing part of the base pairs via protein–DNA interactions, which may lead to higher RMSF values of other base pairs.

### 3.2. Structural Stability and Conformational Transitions of DNA Molecules.

All analyses in this section were performed by excluding the terminal base pairs of DNA due to the end effects (the intermittent breaking of hydrogen bonds and the opening of the terminal base pair).<sup>53–55</sup>

**3.2.1. Structural Stability of DNA Molecules.** To compare the structural changes of both the bound and unbound DNA strands in detailed, the probability distributions of the pyrimidine–purine N1–N3 base pair distances are computed at four different temperatures (Figures S4–S7). The criteria for Watson–Crick (WC)-type base pairing is about 3.5 Å between N1 and N3 atoms, and the distance longer than 5 Å indicates the disruption of base pairs.<sup>22,56</sup> As shown in Figures S4 and S5, nearly all the base pairs in both the bound and unbound DNA molecules maintain base pairing characterized by sharp peaks at 3 Å at 300 and 350 K. However, the A7T2 base pair of the unbound DNA strands from 3LWH starts undergoing base opening at 350 K displaying nonzero probabilities beyond 5 Å. At 400 K (Figure S6), all base pairs of the unbound DNA strands from 3LWH and two specific base pairs (C2G7 and

**Table 2. Percentage (%) of Base Pair Closed States in the MD Simulations on DNA and Protein–DNA Complexes Computed Based on N1–N3 Distances with a Cutoff of 3.5 Å**

	DNA(alone)				DNA(complex)			
	300 K	350 K	400 K	450 K	300 K	350 K	400 K	450 K
<b>3LWH</b>								
T2-A7	99.9	92.5	0.4	0.0	100.0	99.6	96.3	2.7
A3-T6	99.9	96.7	14.7	0.3	99.9	99.7	99.4	19.1
A4-T5	100.0	99.1	12.2	1.7	100.0	99.8	99.6	93.2
T5-A4	99.9	97.9	15.1	0.0	98.8	99.6	99.6	96.2
T6-A3	99.9	95.8	21.4	0.0	99.9	99.7	98.9	84.1
A7-T2	99.4	87.4	0.0	0.0	94.2	92.1	33.6	4.9
<b>3LWI</b>								
C2-G7	100.0	98.6	32.8	0.0	100.0	99.9	99.8	0.3
G3-C6	100.0	99.4	95.8	12.3	100.0	99.8	99.4	0.4
A4-T5	99.8	99.7	99.1	0.0	100.0	99.9	99.5	45.3
T5-A4	99.8	99.6	99.3	17.1	100.0	99.9	99.4	53.1
C6-G3	100.0	99.9	99.2	26.4	100.0	99.9	99.7	53.6
G7-C2	100.0	99.4	96.7	16.1	100.0	100.0	96.7	0.0

G3C6) of the unbound DNA strands from 3LWI undergo base opening, while only one specific base pair (A7T2) exhibits nonzero probabilities beyond 5 Å in 3LWH. At 450 K (Figure S7), all base pairs of the DNA undergo base opening even in the two Cren7–DNA complexes. The above analysis shows the Cren7 protein facilitates stabilization of the DNA in the complex over a certain temperature range. In addition, the percentage of N1–N3 base pair closed states was calculated (Table 2). These data reveal that the WC base pairs are gradually destroyed with the increase in temperature, and the extent of base pair disruption is related to the sequence differences in two DNA molecules. Our simulations show that AT-rich DNA is more prone to denature than the corresponding GC-rich sequence with temperatures rising. This difference should be closely related to the mechanical stiffness in the DNA molecules, which stems from base-stacking interactions and base-pairing hydrogen interactions.

**3.2.2. Conformational Transitions of DNA Molecules.** In our study, the sugar pucker conformation was classified as follows: A-like sugars include the pseudorotation angle (*P*) parameter<sup>57–59</sup> values from −30° to 90° and the B-like sugars include values between 90° and 210°.<sup>60</sup>

The DNA bound by Cren7 protein shows similar conformational change to that bound by Sso7d/Sac7d proteins.<sup>26</sup> To investigate the effect of Cren7 binding and elevated temperatures on the conformation of DNA in the two complexes, the probability distributions of sugar pseudorotation angles for both DNA strands in the two complexes were computed (Table 3). In general, the probability of the B-like form at 350 K is lower than that at 300 K, while the A-like form of the DNA molecules shows the opposite change. However, these probability changes are not significant, which is not quite identical with those in the studies on Sac7d-DNA complexes.<sup>22</sup> We can conjecture that this discrepancy may be relevant to a small kink (~50°) in DNA molecules introduced by Cren7. The three nucleotides (D3a, D3b, and D4b) (Figure 1) in 3LWH and the two nucleotides (D3a and D5a) in 3LWI, which are close to the kink sites, take the A-like sugar conformations, while the four nucleotides (D2a, D4a, D6b, and D7b) in 3LWH and the six nucleotides (D2a, D4a, D6a, D6b, D7a, and D7b) in 3LWI, which locate far away from the kink sites, adopt the B-like sugar conformations. The effect of temperature on the conformational transition of DNA is mainly contributed by the

**Table 3. Percentage (%) of A-like (A) and B-like (B) Conformations for the 12 Individual Nucleotides and the Total 12 Nucleotides in Both Complementary Strands of the Bound DNA at 300 and 350 K**

	3LWH				3LWI			
	300 K		350 K		300 K		350 K	
	A	B	A	B	A	B	A	B
D2a	7.4	92.6	9.3	90.6	8.1	91.8	8.7	91.2
D2b	56.3	43.7	40.7	59.3	21.3	78.7	60.1	38.9
D3a	61.8	38.0	52.3	47.6	68.5	30.7	68.2	31.7
D3b	60.3	39.3	68.9	30.1	34.6	65.4	90.4	8.7
D4a	29.2	70.8	26.9	73.0	34.2	65.8	39.6	60.4
D4b	94.9	2.1	93.8	5.0	66.9	33.0	9.3	90.7
D5a	28.2	71.8	85.2	14.7	75.2	24.8	61.5	38.5
D5b	76.1	23.7	3.1	96.8	58.2	41.7	34.8	65.1
D6a	3.8	96.2	84.6	15.1	4.6	95.3	13.3	86.7
D6b	29.2	70.7	4.1	95.8	28.6	71.4	30.0	69.9
D7a	36.4	63.5	65.6	33.4	44.4	55.6	40.7	59.2
D7b	20.4	79.6	19.8	80.1	10.5	89.5	12.3	87.7
total	42.0	57.7	44.1	55.6	37.9	62.0	40.4	59.5

five nucleotides (D2b, D5a, D5b, D6a, and D7a) in 3LWH and the four nucleotides (D2b, D3b, D4b, and D5b) in 3LWI. These structural transitions of nucleotides may be relevant to the hydrophobic residues.

**3.3. Energetic Analysis of the Two Cren7–DNA Complexes.** **3.3.1. Binding Free Energy Analysis.** The components of the binding free energies for the two Cren7–DNA complexes were computed with MM-PBSA methods. For each of the systems, the snapshot structures used for free energy calculations were extracted from the last 10 ns trajectory. To evaluate the convergence of the simulation, the time evolutions of the RMSD values for the Cren7/DNA systems are shown (Figure S1). As shown in Figure S1, the RMSD plots indicate that all systems achieved equilibrium after about 17 ns at 300 and 350 K. Some of them, such as DNA, seemingly did not reach equilibrium throughout the entire MD simulations at 400 and 450 K. Therefore, we focus on the results from the MD trajectories of the systems at 300 and 350 K. To further test the convergence of the simulation, the time evolution of the enthalpy and the entropy for the two complexes was monitored (Figures 3 and 4). As can be seen

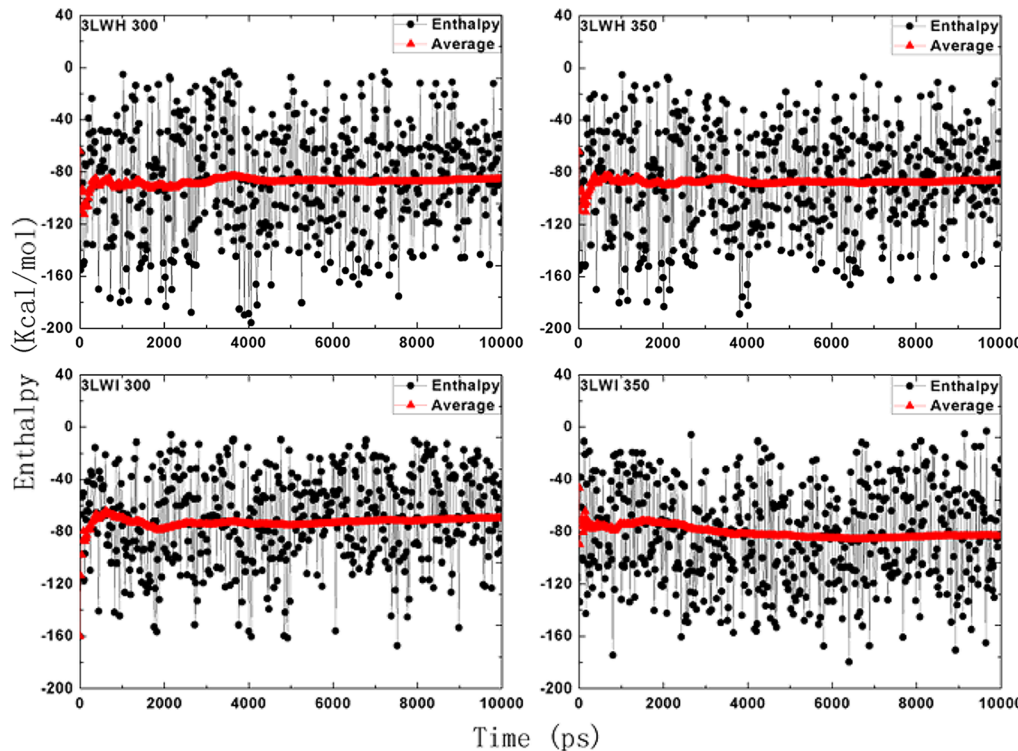


Figure 3. The fluctuations and the accumulated mean values of enthalpies for the two complexes at 300 and 350 K.

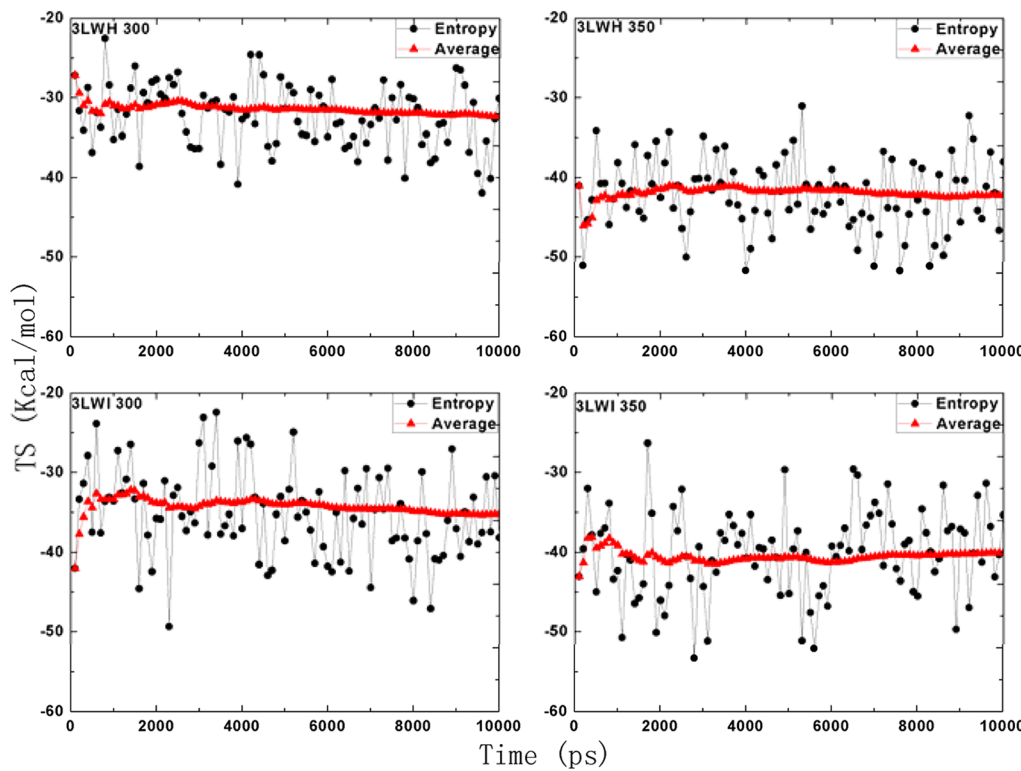


Figure 4. The fluctuations and the accumulated mean values of entropies for the two complexes at 300 and 350 K.

from Figures 3 and 4, the enthalpies and entropies are quite variable, but the averaged values became stable quickly after a short length of MD simulation for the two complexes. From the structural and energetic analysis, we can see that the systems are stable during the last 10 ns MD simulations.

The detailed contributions of various energy components computed by MM-PBSA and the entropy contributions from the normal-mode analysis are given in Table 4. As can be seen in Table 4, the major favorable contributions to the binding free energies ( $G_{\text{bind}}$ ) come from the nonpolar solvation energies ( $G_{\text{np}}$ ), more specifically from the van der Waals energies ( $E_{\text{vdw}}$ ).

**Table 4.** Binding Free Energy and Its Components (kcal/mol) of the 3LWH and 3LWI Complexes Calculated from Triplet-Trajectory Analysis at 300 and 350 K

	3LWH		3LWI	
	300 K	350 K	300 K	350 K
$E_{\text{ele}}$	$-2661.3 \pm 4.75$	$-2753.8 \pm 3.69$	$-2625.0 \pm 4.01$	$-2632.2 \pm 4.62$
$E_{\text{vdw}}$	$-76.5 \pm 0.87$	$-85.9 \pm 0.93$	$-90.7 \pm 0.96$	$-80.9 \pm 0.92$
$G_{\text{nomp}}$	$-8.2 \pm 0.06$	$-8.8 \pm 0.19$	$-8.5 \pm 0.22$	$-8.1 \pm 0.23$
$G_{\text{pb}}$	$2667.1 \pm 3.08$	$2757.6 \pm 4.33$	$2648.4 \pm 3.81$	$2642.4 \pm 4.21$
$E_{\text{int}}$	$4.6 \pm 1.21$	$3.3 \pm 1.43$	$5.9 \pm 1.38$	$3.2 \pm 1.27$
$G_{\text{np}}^a$	$-84.7 \pm 0.81$	$-94.7 \pm 1.31$	$-99.2 \pm 1.47$	$-89.0 \pm 1.11$
$G_{\text{pb}}^b$	$5.8 \pm 0.27$	$3.8 \pm 1.12$	$23.4 \pm 1.94$	$10.2 \pm 1.67$
$E_{\text{MM}}$	$-2733.2 \pm 3.82$	$-2836.4 \pm 4.25$	$-2709.8 \pm 3.35$	$-2716.3 \pm 4.92$
$G_{\text{solv}}$	$2659.0 \pm 5.19$	$2748.9 \pm 4.61$	$2639.9 \pm 3.78$	$2634.3 \pm 4.59$
$H$	$-74.3 \pm 1.82$	$-87.6 \pm 1.34$	$-70.0 \pm 1.96$	$-82.0 \pm 2.44$
$-\text{TS}$	$32.1 \pm 0.68$	$42.8 \pm 0.77$	$35.3 \pm 0.82$	$41.1 \pm 0.71$
$G_{\text{bind}}^c$	$-42.2 \pm 1.24$	$-48.6 \pm 1.85$	$-34.7 \pm 1.29$	$-40.9 \pm 1.63$

<sup>a</sup> $G_{\text{np}} = E_{\text{vdw}} + G_{\text{nomp}}$ . <sup>b</sup> $G_{\text{pb}} = E_{\text{ele}} + G_{\text{pb}}$ . <sup>c</sup> $G_{\text{bind}} = G_{\text{nomp}} + G_{\text{pb}} + E_{\text{int}} - \text{TS}$ .

In contrast to the nonpolar solvation energies ( $G_{\text{np}}$ ), the polar solvation energies ( $G_{\text{pb}}$ ) make unfavorable contribution to the binding energy. Actually, the direct intermolecular electrostatic interactions ( $E_{\text{ele}}$ ) are highly favorable to the binding but their contributions are completely screened by the unfavorable stronger polar-electrostatic solvation energies ( $G_{\text{pb}}$ ). In addition, the contributions of entropy changes ( $-\text{TS}$ ) to the free energies impair the binding of the two DNA molecules to protein Cren7. In general, the favorable van der Waals ( $E_{\text{vdw}}$ ) and nonelectrostatic solvation interactions energies ( $G_{\text{nomp}}$ ) mainly drive the binding between the Cren7 protein and DNA in 3LWH and 3LWI. The binding free energies for 3LWH and 3LWI are estimated to be  $-42.2$  and  $-34.7$  kcal/mol at 300 K and  $-48.6$  and  $-40.9$  kcal/mol at 350 K, respectively, showing a similar trend compared with the experimental results of two Sul7 proteins.<sup>61–63</sup> These energies at 350 K are lower than those at 300 K, indicating the binding is stronger in 3LWH and 3LWI at 350 K.

A much better understanding of the protein–DNA recognition is obtained via the interaction energy analysis. The attractive interactions between Cren7 protein and the phosphate backbone are stronger than the corresponding interactions between the protein and the bases of nucleotides (Table S1). The energy analysis, along with the visual inspection of both binary MD and crystal structures, indicates that the interaction energies of DNA and Cren7 are dominated by electrostatic energies between Cren7 and DNA phosphate backbone. This leads to the conclusion that the Cren7 is a nonsequence specific DNA binding protein, which is consistent with the results from experiments.<sup>26</sup>

**3.3.2. Per-Residue Free Energy Decomposition.** In order to characterize and identify the key residues of the Cren7–DNA interaction interface in 3LWH and 3LWI, per-residue free energy decomposition was performed (Figure 5). The values of  $\Delta G_{\text{MM+solv}}$  were decomposed on a per-residue basis into contributions from internal energy, van der Waals energy, Coulombic interactions energy, polar solvation free energy, and the nonpolar solvation free energy. These residues with  $|\Delta G_{\text{MM+solv}}| \geq 1.0$  kcal/mol free energy were listed in Tables S2–S5. Seven amino acid residues (Lys24, Trp26, Leu28, Pro30, Lys31, Arg51, and Lys53) make major contributions to the binding free energy with more than 3.5 kcal/mol free energy for 3LWH and 3LWI (Figure 5). These residues are very important for the Cren7–DNA binding, which are in good

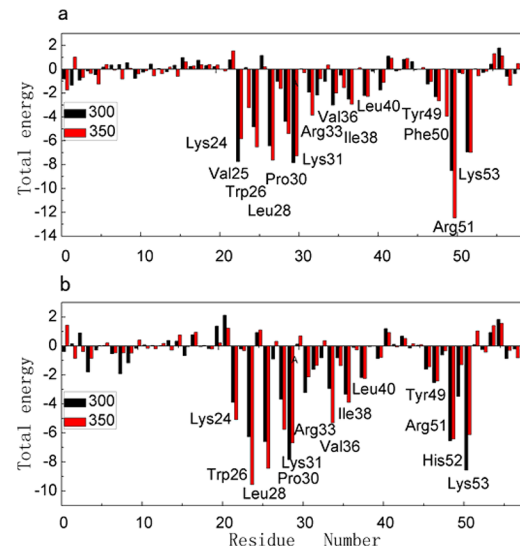


**Figure 5.** Free energy decomposition analysis at 300 and 350 K for 3LWH (a) and 3LWI (b); residues contributing significantly are highlighted.

agreement with the previous experimental identification.<sup>26,27</sup> As seen from Tables S2–S5, some other residues (Arg33, Val36, Ile38, Leu40, and Tyr49) are important in DNA binding with more than 2 kcal/mol free energy contribution. Mutation of those residues to Ala results in drastically increased dissociation rates and the lowest affinity for DNA, which shows that these amino acid residues play a critical role in stabilizing the Cren7–DNA complex.<sup>26</sup> Compared with the decomposition energies of residues at 300 K, the decomposition energies of the three amino acid residues (Trp26, Leu28, and Pro30) are increased at 350 K (Tables S2–S5), indicating a larger contribution of conserved residues to the stability of the two complexes. Although the decomposition energy of Lys24, Lys31, Arg51, and Lys53 is not increased at 350 K, it has a significantly favorable contribution to the binding free energy. This analysis shows that these three residues also play a critical role in stabilizing this protein–DNA complex.

In addition, the binding free energies for the two Cren7–DNA complexes mainly come from one strand of DNA molecules (Tables S2–S5), which indicates that the Cren7 protein interacts favorably with one strand of the DNA. This

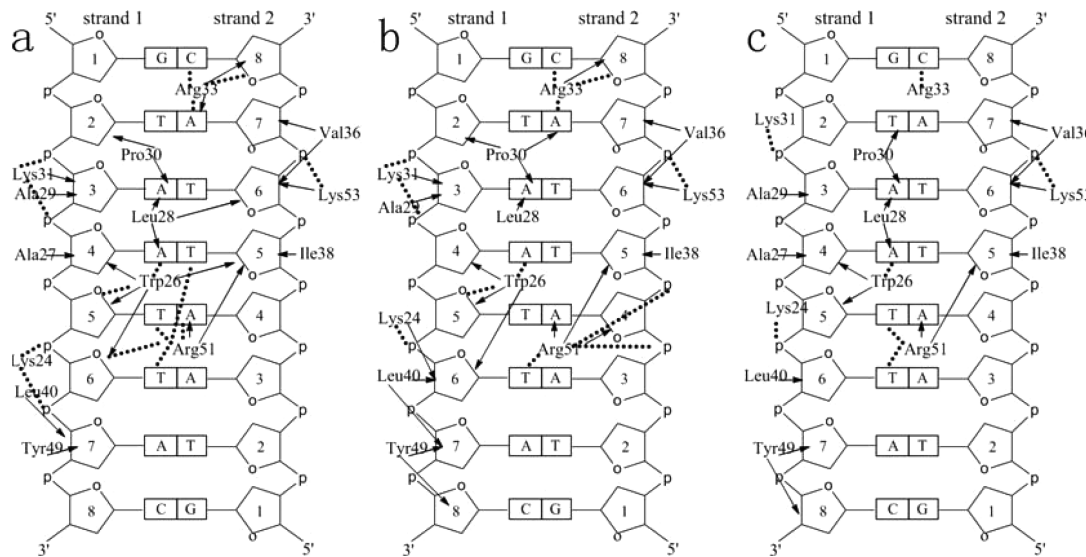


**Figure 6.** Diagrams of the calculated key contact sites of Cren7 with DNA at 300 (a) and 350 K (b) compared with the corresponding experimental results (c) for 3LWH. Hydrogen bonds and hydrophobic interactions are shown with dashed lines and arrows, respectively.

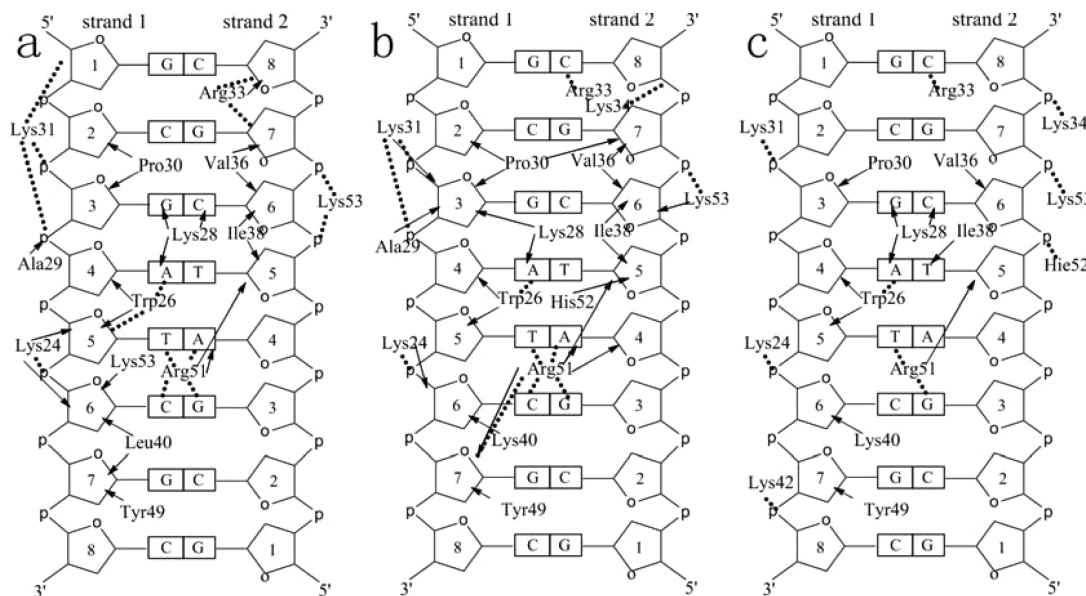


**Figure 7.** Diagrams of the calculated key contact sites of Cren7 with DNA at 300 (a) and 350 K (b) compared with the corresponding experimental results (c) for 3LWI. Hydrogen bonds and hydrophobic interactions are shown with dashed lines and arrows, respectively.

result can also be verified by hydrogen bonds and hydrophobic interactions during the MD process.

From Tables S2–S5, it can be seen that most of the important residues for both 3LWH and 3LWI have a large van der Waals interaction contribution while the polar interaction has a relatively small influence. But for some of the other residues, the polar interactions also have an obvious contribution, for example, Lys24, Lys53, and so on. Most of these polar interactions stem from the formation of hydrogen bonds. The detailed interaction between Cren7 protein and DNA can be observed by monitoring the occupation probability of these hydrogen bonds and hydrophobic interactions during the MD process.

### 3.4. Cren7–DNA Interactions and Simulations Result Comparison with Experiments Data.

The protein–DNA interactions were investigated with the focus on hydrogen bonds and hydrophobic interactions. The criteria for hydrogen-

bonded pairs are the distance shorter than 3.5 Å and the binding angle greater than 120.0° between the hydrogen donor and acceptor atoms. The hydrophobic contact is defined as a distance between carbon atoms shorter than 4.5 Å<sup>64</sup> in our work.

**3.4.1. Protein–DNA Hydrogen Bonds Analysis.** Hydrogen-bonding interactions between Cren7 protein and the two DNA molecules were listed in Tables S6 and S7 when the contacts populated over 20% during the last 20 ns of simulations for 3LWH and 3LWI. Protein–DNA hydrogen bonds include both nonspecific interactions (between Cren7 and DNA sugar/phosphate backbone), being significant for the stability of protein–DNA complex, and specific interactions (between Cren7 and DNA base), being important to the molecular recognition process in protein–DNA complex.

Amino acids in Cren7, including Lys31 and Arg33 in  $\beta$ 3– $\beta$ 4 loop, Lys24 and Trp26 in  $\beta$ 3, and Arg51 and Lys53 in  $\beta$ 5, are

involved in the stable hydrogen bonds between Cren7 and DNA at 300 and 350 K for 3LWH (Figure 6a,b and Table S6). These hydrogen bond interactions mentioned above have also been reported by experimental studies (Figure 6c). In addition to these interactions reported by experimental studies,<sup>26</sup> these amino acids also participate in other hydrogen bond contacts with DNA in our simulations. In detail, amino acid Arg51 is involved in an extensive network of hydrogen bonds with 1T5, 2T5, and 2A4. The H<sub>Z</sub> atom of Lys26 forms hydrogen bonds with 1A7. Residues Trp24, Lys31, Arg33, and Lys53 are involved in the hydrogen bond interactions with the DNA molecule. In a word, the hydrogen bonds with the DNA bases concentrate on the central three base pairs (A4T5, TSA4, and T6A3) of the DNA molecules in 3LWH. These hydrogen bond interactions are from Trp26 and Arg51. However, Arg51 mainly forms hydrogen bonds with the DNA sugar/phosphate backbone at 350 K, which probably contributes to structural transitions of the DNA molecule.

As can be seen from panels a and b of Figure 7 and Table S7, residues Lys24, Trp26, Lys31, Arg33, Arg51, and Lys53 are involved in stable hydrogen bonds between Cren7 and DNA at 300 and 350 K for 3LWI, which are consistent with the experimental results<sup>27</sup> (Figure 7c). In addition to these crucial interactions, some hydrogen bonds are not identified by previous experiment. In detail, the residues Trp26, Lys31, Arg33, and Arg51 of Cren7 protein were involved in hydrogen bond interactions with DNA, while the residues Lys32 and Lys42 are not involved in the hydrogen bond interactions with DNA in comparison with experimental data determined for 3LWI.<sup>27</sup> These disparities were likely to result from the fact that the other types of interactions occur in those residues, such as the electrostatic and hydrophobic interactions. The observations above indicate that the number of hydrogen bonds formed at 350 K is less than that at 300 K, which is in accord with the result of the binding free energy computed.

**3.4.2. Protein–DNA Hydrophobic Analysis.** The hydrophobic distance analysis was performed for the 3LWH (Figure 6a,b and Table S8). The hydrophobic interactions exist between these partners (Leu28 and base pairs 1A3–1A4, Trp26 and base pairs 1A4–1T5, Ala29 and base pair 1A3, Lys51 and base pairs 2T4–2A5, Tyr49 and base pair 1T7, Val36 and base pairs 2A2–2T3, Pro30 and base pair 1A3, Leu40 and base pair 1T6, and Ile38 and base pair 2T4) at 300 and 350 K. These hydrophobic interactions have also been reported by the experimental investigations<sup>26</sup> as shown in Figure 6c. Hydrophobic interactions on the DNA bases are located on the three base pairs (T2A7, A3T6, and A4T5). The roll at T2pA3 and A3pA4 steps may result from the hydrophobic interactions of Leu28 and Pro30 with these bases.

The hydrophobic distance analysis for the 3LWI suggests that the residues Trp26, Leu28, Arg51, Ala29, Val36, Pro30, Tyr49, Ile38, and Leu40 are involved in hydrophobic interactions (Figure 7a,b and Table S9). These hydrophobic interactions form the network of van der Waals interactions, which has been reported by the experimental investigations<sup>27</sup> as shown in Figure 7c. The probability distribution corresponding to these hydrophobic interactions exhibits various contacts in MD simulations at the two temperatures (300 and 350 K). Therefore, these hydrophobic interactions may facilitate structural transitions of nucleotides. The hydrophobic sites for 3LWI at 350 K are more than those at 300 K (Table S9), which is consistent with the decrement of the binding free energy.

## 4. CONCLUSION

Focused on the two specific Cren7–DNA complexes (PDB codes 3LWH and 3LWI), we performed MD simulations at four different temperatures (300, 350, 400, and 450 K) to investigate the thermal stability and structural transitions of DNA depending on temperature. Furthermore, MM-PBSA at 300 and 350 K was used to analyze the detailed interaction and binding free energy in the two complexes.

The results from MD simulations indicate that DNAs in alone systems are more prone to denature than those in complexes with temperature increasing. At 300 K, the DNA molecules in MD simulations of unbound DNA and Cren7–DNA complexes are nearly unchanged in comparison with the experimental structures. At 350 K, slight structural changes of the DNA molecules in the two complexes were observed; however, unbound DNAs are more flexible and were found to display base opening. At 400 K, about 60% base pairs undergo base opening in the unbound DNA, while about 95% base pairs still remain stable in the two complexes. At the extreme high temperature of 450 K, the DNA molecules undergo denaturation completely in the simulations of unbound DNA; however, a small percentage of base pairs still remain stable in the presence of the protein. On the whole, the protein Cren7 can help to stabilize the DNA molecules within a certain temperature range. In addition to the thermal stability, the DNA molecules in the two complexes also undergo B-like to A-like form transitions with increased temperature; however, this transition only occurs in five nucleotides (D2b, D5a, D5b, D6a, and D7a) in 3LWH and four nucleotides (D2b, D3b, D4b, and D5b) in 3LWI.

MM-PBSA free energy calculations provide the following energetic information: (1) the binding affinity for both the 3LWH and 3LWI complexes shows an increasing trend as temperatures rise, which is consistent with the experimental results of the two Sul7 proteins, (2) the extensive interactions between Cren7 and DNA phosphate backbones are the reason nonspecific DNA-binding protein Cren7 is proposed, and (3) the dominant contribution to the binding free energy of the two complexes comes from the van der Waals interaction and seven conserved amino acid residues (Lys24, Trp26, Leu28, Pro30, Lys31, Arg51, and Lys53) make major contributions for Cren7–DNA binding. Furthermore, the hydrogen bonds and hydrophobic analysis suggest that four residues (Trp26, Leu28, Pro30, and Arg51) have significant influence on the structure of DNA molecules, and the hydrogen bonds and hydrophobic interactions at Cren7 protein and DNA interface have been identified at the key contact sites for the two complexes, which is consistent with the results from experiments.<sup>26,27</sup>

MD simulations and MM-PBSA calculations provide the above dynamic structural information and energetic information, which are often inaccessible in the static crystal structure. This study will lead to a better understanding of Cren7–DNA interactions.

## ■ ASSOCIATED CONTENT

### S Supporting Information

**Table S1.** Interaction energies of Cren7–DNA-base and Cren7–DNA-backbone (Table S1); relative binding free energies contributed by important residues ( $|\Delta G_{\text{bind}}| \geq 1.0 \text{ kcal mol}^{-1}$ ) in 3LWH complex at 300 K (Table S2); relative binding free energies contributed by important residues ( $|\Delta G_{\text{bind}}| \geq 1.0 \text{ kcal mol}^{-1}$ ) in 3LWH complex at 350 K

(Table S3); relative binding free energies contributed by important residues ( $|\Delta G_{\text{bind}}| \geq 1.0 \text{ kcal mol}^{-1}$ ) in 3LWI complex at 300 K (Table S4); relative binding free energies contributed by important residues ( $|\Delta G_{\text{bind}}| \geq 1.0 \text{ kcal mol}^{-1}$ ) in 3LWI complex at 350 K (Table S5); hydrogen bond analysis for 3LWH complex at 300 and 350 K (Table S6); hydrogen bond analysis for 3LWI complex at 300 and 350 K (Table S7); hydrophobic analysis for the 3LWH complex at 300 and 350 K (Table S8); hydrophobic analysis for the 3LWI complex at 300 and 350 K (Table S9); time dependence of the RMSD values of molecules investigated in the present paper from the initial structures extracted from the two Cren7–DNA complexes at four different temperatures (Figure S1); snapshots of the three-dimensional structures of Cren7 during the free protein simulations at 450 K and the corresponding time of the each representative conformation (Figure S2); contact maps indicating the inter-residue/nucleotide distances that were calculated and plotted over the last 20 ns of the simulations on the 3LWH and 3LWI complexes at different temperatures (Figure S3); probability distributions of the N1(G/A)–N3(C/T) distances in the central six base pairs of the unbound DNA and bound DNA systems at 300 K (Figure S4); probability distributions of the N1(G/A)–N3(C/T) distances in the central six base pairs of the unbound DNA and bound DNA systems at 350 K (Figure S5); probability distributions of the N1(G/A)–N3(C/T) distances in the central six base pairs of the unbound DNA and bound DNA systems at 400 K (Figure S6); and probability distributions of the N1(G/A)–N3(C/T) distances in the central six base pairs of the unbound DNA and bound DNA systems at 450 K (Figure S7). This material is available free of charge via the Internet at <http://pubs.acs.org>.

## AUTHOR INFORMATION

### Corresponding Author

\*Tel: +86-431-88498962. Fax: +86-431-88498962. E-mail: zhengqc@jlu.edu.cn and zhanghx@mail.jlu.edu.cn.

### Notes

The authors declare no competing financial interest.

## ACKNOWLEDGMENTS

This work is supported by Natural Science Foundation of China and Specialized Research Fund for the Doctoral Program of Higher Education (Grant Nos. 21273095, 20903045, 21203072, and 20070183046).

## REFERENCES

- (1) Dickerson, R. E. *Nucleic Acids Res.* **1998**, *26*, 1906–1926.
- (2) Kalodimos, C. G.; Biris, N.; Bonvin, A. M. J. J.; Levandoski, M. M.; Guennuegues, M.; Boelens, R.; Kaptein, R. *Science* **2004**, *305*, 386–389.
- (3) MacBeath, G. *Nat. Genet.* **2002**, *32*, 526–532.
- (4) Storto, G. D.; Fields, D. S. *Trends Biochem. Sci.* **1998**, *23*, 109–113.
- (5) Todorova, R.; Atanasov, B. *Int. J. Biol. Macromol.* **2004**, *34*, 135–147.
- (6) Sandman, K.; Reeve, J. N. *Curr. Opin. Microbiol.* **2005**, *8*, 656–661.
- (7) Choli, T.; Wittmann-Liebold, B.; Reinhardt, R. *J. Biol. Chem.* **1988**, *263*, 7087–7093.
- (8) Grote, M.; Dijk, J.; Reinhardt, R. *Biochim. Biophys. Acta, Protein Struct. Mol. Enzymol.* **1986**, *873*, 405–413.
- (9) Kimura, M.; Kimura, J.; Davie, P.; Reinhardt, R.; Dijk, J. *FEBS Lett.* **1984**, *176*, 176–178.
- (10) Gao, Y. G.; Su, S. Y.; Robinson, H.; Padmanabhan, S.; Lim, L.; McCrary, B. S.; Edmondson, S. P.; Shriner, J. W.; Wang, A. H. *J. Nat. Struct. Mol. Biol.* **1998**, *5*, 782–786.
- (11) Bruins, M. E.; Janssen, A. E. M.; Boom, R. M. *Appl. Biochem. Biotechnol.* **2001**, *90*, 155–186.
- (12) Turner, P.; Mamo, G.; Karlsson, E. N. *Microb. Cell Fact* **2007**, *6*, 1–23.
- (13) Ciaramella, M.; Pisani, F. M.; Rossi, M. *Antonie Van Leeuwenhoek* **2002**, *81*, 85–97.
- (14) She, Q.; Singh, R. K.; Confalonieri, F.; Zivanovic, Y.; Allard, G.; Awayez, M. J.; Chan-Weiher, C. C. Y.; Clausen, I. G.; Curtis, B. A.; De Moors, A. *Proc. Natl. Acad. Sci. U.S.A.* **2001**, *98*, 7835.
- (15) Bernander, R. *Mol. Microbiol.* **2007**, *66*, 557–562.
- (16) Shriner, J. W.; Peters, W. B.; Szary, N.; Clark, A. T.; Edmondson, S. P. *Methods Enzymol.* **2001**, *334*, 389–422.
- (17) Edmondson, S. P.; Shriner, J. W. *Methods Enzymol.* **2001**, *334*, 129–145.
- (18) Guo, L.; Feng, Y.; Zhang, Z.; Yao, H.; Luo, Y.; Wang, J.; Huang, L. *Nucleic Acids Res.* **2008**, *36*, 1129–1137.
- (19) Priyakumar, U. *J. Biomol. Struct. Dyn.* **2012**, *29*, 961–971.
- (20) Gera, N.; Hussain, M.; Wright, R. C.; Rao, B. M. *J. Mol. Biol.* **2011**, *409*, 601–616.
- (21) Andrea, B.; Ottavia, S.; Roberto, C.; Ivana, A.; Paola, F.; Simone, C.; Annamaria, G.; Neri, N. *BMC Struct. Biol.* **2011**, *11*, 44.
- (22) Priyakumar, U. D.; Harika, G.; Suresh, G. *J. Phys. Chem. B* **2010**, *114*, 16548–16557.
- (23) Priyakumar, U. D.; Ramakrishna, S.; Nagarjuna, K.; Reddy, S. K. *J. Phys. Chem. B* **2010**, *114*, 1707–1718.
- (24) Xu, X.; Su, J.; Chen, W.; Wang, C. *J. Biomol. Struct. Dyn.* **2011**, *28*, 717–727.
- (25) Bell, S. D.; White, M. F. *Bacterial Chromatin* **2010**, 205–217.
- (26) Zhang, Z.; Gong, Y.; Guo, L.; Jiang, T.; Huang, L. *Mol. Microbiol.* **2010**, *76*, 749–759.
- (27) Feng, Y.; Yao, H.; Wang, J. *Protein Sci.* **2010**, *19*, 1253–1257.
- (28) Liu, H.; Yao, X. *Mol. Pharmaceutics* **2009**, *7*, 75–85.
- (29) Lee, J.; Kim, J. S.; Seok, C. *J. Phys. Chem. B* **2010**, *114*, 7662–7671.
- (30) Gohlke, H.; Kiel, C.; Case, D. A. *J. Mol. Biol.* **2003**, *330*, 891–913.
- (31) Bahadur, R. P.; Kannan, S.; Zacharias, M. *Biophys. J.* **2009**, *97*, 3139–3149.
- (32) Hou, T.; Li, N.; Li, Y.; Wang, W. *J. Proteome Res.* **2012**, *11*, 2982–2995.
- (33) Case, D.; Darden, T.; Cheatham, T., III; Simmerling, C.; Wang, J.; Duke, R.; Luo, R.; Crowley, M.; Walker, R. C.; Zhang, W.; et al. *Amber 10*; University of California: San Francisco, CA, 2008, p 32.
- (34) Duan, Y.; Wu, C.; Chowdhury, S.; Lee, M. C.; Xiong, G.; Zhang, W.; Yang, R.; Cieplak, P.; Luo, R.; Lee, T. *J. Comput. Chem.* **2003**, *24*, 1999–2012.
- (35) Qin, F.; Jiang, Y.; Chen, Y.; Wu, M.; Yan, G.; Ye, W.; Li, Y.; Zhang, J.; Chen, H. F. *Phys. Chem. Chem. Phys.* **2011**, *13*, 1407–1412.
- (36) Jorgensen, W. L.; Chandrasekhar, J.; Madura, J. D.; Impey, R. W.; Klein, M. L. *J. Chem. Phys.* **1983**, *79*, 926.
- (37) Darden, T.; York, D.; Pedersen, L. *J. Chem. Phys.* **1993**, *98*, 10089–10092.
- (38) Ryckaert, J. P.; Ciccotti, G.; Berendsen, H. J. C. *J. Comput. Phys.* **1977**, *23*, 327–341.
- (39) DeLano, W. L. *The PyMOL User's Manual*; DeLano Scientific: San Carlos, CA, 2002, p 382.
- (40) Humphrey, W.; Dalke, A.; Schulten, K. *J. Mol. Graphics* **1996**, *14*, 33–38.
- (41) Srinivasan, J.; Cheatham, T. E., III; Cieplak, P.; Kollman, P. A.; David, A. *J. Am. Chem. Soc.* **1998**, *120*, 9401–9409.
- (42) Swanson, J. M. J.; Henchman, R. H.; McCammon, J. A. *Biophys. J.* **2004**, *86*, 67–74.
- (43) Hou, T.; Wang, J.; Li, Y.; Wang, W. *J. Chem. Inf. Model.* **2011**, *51*, 69–82.

- (44) Case, D.; Darden, T.; Cheatham, T.; Simmerling, C.; Wang, J.; Duke, R.; Luo, R.; Walker, R.; Zhang, W.; Merz, K. M.; et al. *Amber* 11; University of California: San Francisco, CA, 2010.
- (45) Bashford, D.; Case, D. A. *Annu. Rev. Phys. Chem.* **2000**, *51*, 129–152.
- (46) Luo, R.; David, L.; Gilson, M. K. *J. Comput. Chem.* **2002**, *23*, 1244–1253.
- (47) Yang, B.; Zhu, Y.; Wang, Y.; Chen, G. *J. Comput. Chem.* **2011**, *32*, 416–428.
- (48) Milev, S.; Gorfe, A. A.; Karshikoff, A.; Clubb, R. T.; Bosshard, H. R.; Jelesarov, I. *Biochemistry* **2003**, *42*, 3481–3491.
- (49) Sitkoff, D.; Sharp, K. A.; Honig, B. *J. Phys. Chem.* **1994**, *98*, 1978–1988.
- (50) Cheatham, T. E.; Srinivasan, J.; Case, D. A.; Kollman, P. A. *J. Biomol. Struct. Dyn.* **1998**, *16*, 265–280.
- (51) Gouda, H.; Kuntz, I. D.; Case, D. A.; Kollman, P. A. *Biopolymers* **2003**, *68*, 16–34.
- (52) Case, D. A. *Curr. Opin. Struct. Biol.* **1994**, *4*, 285–290.
- (53) Marathe, A.; Bansal, M. *J. Phys. Chem. B* **2010**, *114*, 5534–5546.
- (54) Leroy, J. L.; Kochoyan, M.; Huynh-Dinh, T.; Guéron, M. *J. Mol. Biol.* **1988**, *200*, 223–238.
- (55) Nonin, S.; Leroy, J. L.; Gueron, M. *Biochemistry* **1995**, *34*, 10652–10659.
- (56) Bueren-Calabuig, J. A.; Giraudon, C.; Galmarini, C. M.; Egly, J. M.; Gago, F. *Nucleic Acids Res.* **2011**, *39*, 8248–8257.
- (57) Cremer, D.; Pople, J. *J. Am. Chem. Soc.* **1975**, *97*, 1354–1358.
- (58) Harvey, S. C.; Prabhakaran, M. *J. Am. Chem. Soc.* **1986**, *108*, 6128–6136.
- (59) Saenger, W. *Principles of nucleic acid structure*; Springer-Verlag: New York, 1984.
- (60) Tolstorukov, M. Y.; Jernigan, R. L.; Zhurkin, V. B. *J. Mol. Biol.* **2004**, *337*, 65–76.
- (61) Chen, L.; Zheng, Q. C.; Yu, L. Y.; Chu, W. T.; Zhang, J. L.; Xue, Q.; Zhang, H. X.; Sun, C. C. *J. Biomol. Struct. Dyn.* **2012**, *30*, 716–727.
- (62) Peters, W. B.; Edmondson, S. P.; Shriver, J. W. *J. Mol. Biol.* **2004**, *343*, 339–360.
- (63) Lundbäck, T.; Hansson, H.; Knapp, S.; Ladenstein, R.; Härd, T. *J. Mol. Biol.* **1998**, *276*, 775–786.
- (64) Gutmanas, A.; Billeter, M. *Proteins: Struct., Funct., Bioinf.* **2004**, *57*, 772–782.